Reduced Dimensionality in Organic Electro-Optic Materials: Theory and Defined Order

Stephanie J. Benight, Lewis E. Johnson, Robin Barnes, Benjamin C. Olbricht, Denise H. Bale, Philip J. Reid, Bruce E. Eichinger, Larry R. Dalton, Philip A. Sullivan, and Bruce H. Robinson*

Department of Chemistry, University of Washington, Seattle, Washington 98195

Received: March 11, 2010; Revised Manuscript Received: July 14, 2010

Identification of electronic intermolecular electrostatic interactions that can significantly enhance poling-induced order is important to the advancement of the field of organic electro-optics. Here, we demonstrate an example of such improvement achieved through exploitation of the interaction of coumarin pendant groups in chromophore-containing macromolecules. Acentric order enhancement is explained in terms of lattice-symmetry effects, where constraint of orientational degrees of freedom alters the relationship between centrosymmetric and acentric order. We demonstrate both experimentally and theoretically that lattice dimensionality can be defined using the relationship between centrosymmetric order and acentric order. Experimentally: Acentric order is determined by attenuated total reflection measurement of electro-optic activity coupled with hyper-Rayleigh scattering measurement of molecular first hyperpolarizability, and centrosymmetric order is determined by the variable angle polarization referenced absorption spectroscopy method. Theoretically: Order is determined from statistical mechanical models that predict the properties of soft condensed matter.

Introduction

Organic electro-optic (EO) materials have the potential to minimize the size, weight, and power requirements of next-generation computing, telecommunications, and sensing applications through dramatically improved performance and simplified processing compared to existing technologies.[1] Creating materials suitable for such applications requires optimization of the EO coefficient, r_{33}, which is the dominant element of the third rank EO tensor and is related to order and hyperpolarizability by

$$r_{33} = 2N\beta_{zzz}(\omega, \varepsilon)\langle\cos^3\theta\rangle\left\{\frac{g(\omega)}{n_\omega^4}\right\} \quad (1)$$

Here, the parameter n_ω is the refractive index of the material. N is the number density of the EO active molecules (chromophores) within the material matrix. $\beta_{zzz}(\omega, \varepsilon)$ is the molecular second-order polarizability (first-order hyperpolarizability; dependent on both the frequency of the optical field, ω, and dielectric constant, $\varepsilon(\omega)$) of the individual EO chromophores. $\langle\cos^3\theta\rangle$ is the molecular acentric order parameter with respect to the poling (z) axis (where θ is the angle between the chromophore dipole and the poling field), and $g(\omega)$ includes the Lorentz−Onsager local field factor. From eq 1, it is evident that r_{33} is dependent on three main parameters: N, $\beta_{zzz}(\omega, \varepsilon)$, and $\langle\cos^3\theta\rangle$, which may be optimized through improved material design.

Simultaneous optimization of these parameters is required to realize improved EO activity. A substantial amount of success has been achieved toward optimizing and understanding $\beta_{zzz}(\omega, \varepsilon)$ through theoretical and experimental research;[1−20] however, realization of molecular/supramolecular architectures that favor high, long-range acentric order in glassy materials remains a fundamental challenge. Glassy, organic electro-optic materials are initially spin-cast from solution to create thin films of isotropically dispersed EO-active chromophores contained within a host matrix. Inducing a significant degree of acentric alignment in these materials requires the application of external ordering force(s), such as electric or optical poling fields and optimization of the dipolar ordering response to these fields. Such a response is typically quantified by the poling efficiency, r_{33}/E_p.

Achieving stable poled materials with high degrees of acentric order has proven difficult.[1,21] Although a number of methods have been explored to produce acentric molecular lattices, electric field poling of an initially isotropic, dipolar chromophore in polymer guest/host material has remained the most heavily studied. Poled materials have the advantage of homogeneity and good optical properties over a large area without elaborate processing (i.e., they facilitate low-loss, low-cost device production); however, energetically favorable antiparallel dipole−dipole interactions increase as chromophore number density increases. Such interactions impede acentric ordering during poling, which limits the chromophore number density required to achieve a maximum value for $N\langle\cos^3\theta\rangle$ (loading parameter).[21,1,22,23]

Several recent reports have confirmed that a number of approaches are effective in managing interchromophore electrostatic (dipole−dipole) interactions. These approaches have allowed chromophore number densities to be pushed to values as high as 7×10^{20} molecules/cc (~50% weight/weight) by employing supramolecular engineering schemes aimed toward the goal of chromophore−chromophore isolation (e.g., site isolation).[20,24−35] Site isolation schemes rely on the use of non-chromophore entities (e.g., dendrons), matrix architecture, or both to physically isolate chromophores using steric effects. This strategy effectively limits the minimum interchromophore approach distance, reducing the electrostatic interactions and thereby improving $N\langle\cos^3\theta\rangle$. In addition to conceptually simple site isolation, careful engineering of directed interactions can be used to enhance acentric chromophore alignment and create an ordered supramolecular lattice environment.[36] Recent studies

* Corresponding author. E-mail: robinson@chem.washington.edu.

10.1021/jp1022423
Published on Web 08/23/2010

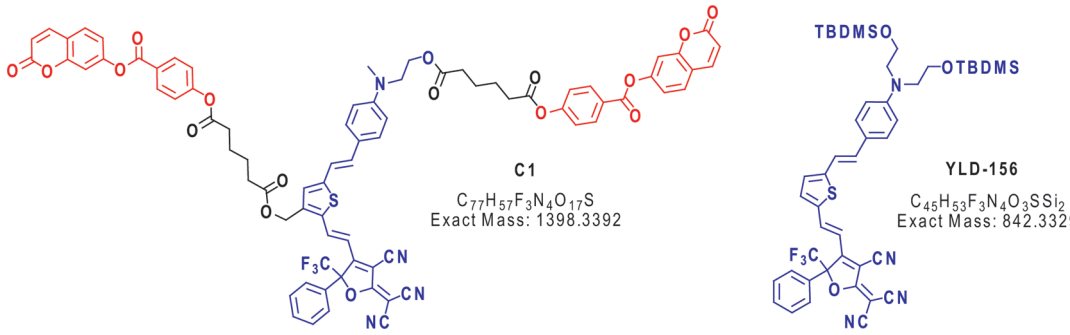

Figure 1. The monolithic (neat) pendant-modified chromophore material, C1 (left), with the chromophore highlighted in blue and pendant groups highlighted in red. The analogous free chromophore, F2, used in the preparation of simple guest/host materials for comparison is shown on the right.

have also shown that an external optical field may be used to enhance guest order by selectively modifying the order of the host matrix.[37]

The work presented here demonstrates an effective method of enhancing $N\langle\cos^3\theta\rangle$ by constraining the number of orientational possibilities available to individual chromophores during the poling process. Noncovalent "soft" intermolecular interactions between chromophore pendant groups are used to create a more ordered matrix in which the chromophores are embedded. This results in enhanced acentric chromophore order along the z-axis (poling) direction in response to the applied electric field (E_p). The dimensionality, or orientational degrees of freedom available to the system, can be quantified by means of the relationship between centrosymmetric and acentric order. A neat chromophore material (C1) bearing pendant groups designed to create directed supramolecular interactions was prepared (Figure 1). Experimental and theoretical analysis of the poling and ordering behavior of C1 and the analogous chromophore F2 (reported previously as YLD-156[38] and shown in Figure 1) poled in a commonly used polymer host, poly(methyl methacrylate) (PMMA), is reported.

Theory

The dimensionality of a material as a function of centrosymmetric and acentric order can be derived through an extension of the independent particle assumption used for calculating such order parameters in the low-density limit. We first define the order parameters $\langle\cos^n\theta\rangle$ with respect to the poling axis associated with an ensemble of independent dipolar chromophores by means of the ratio[22]

$$\langle\cos^n\theta\rangle = \frac{\iint_{\theta,\phi}\cos^n\theta\, P(\theta,\phi)\, e^{\mu\cdot E_0/kT}\,\mathrm{d}\cos\theta\,\mathrm{d}\phi}{\iint_{\theta,\phi}P(\theta,\phi)\, e^{\mu\cdot E_0/kT}\,\mathrm{d}\cos\theta\,\mathrm{d}\phi} \quad (2)$$

The probability distribution, $P(\theta,\phi) = (1/Z_0)e^{-(H_0/kT)}$, is determined by the underlying many-body interaction potential (Hamiltonian). This complicated probability distribution is modeled here by a uniform potential in a space of reduced dimensionality. The term $e^{\mu\cdot E_0/kT}$ is the statistical weight associated with the interaction of the dipole with a homogeneous poling field, E_0. This field, E_0, is defined at the location of the molecule and related to the macroscopic field, E, by the electrostatic boundary conditions of the system.[39,40] The presence of an external poling field perturbs the overall distribution but can be treated as an additive contribution to the Hamiltonian.

Now consider that the underlying probability distribution gives a uniform distribution in a space of one, two, or three dimensions. In three dimensions, the dipole may access any orientation by rotating about the origin with respect to all three Cartesian axes. The order parameters are found from the expression

$$\langle\cos^n\theta\rangle_{3D} = L_n(f) = \frac{\iint_{\theta,\phi}\cos^n\theta\, e^{\vec{\mu}\cdot\vec{E}_0/kT}\,\mathrm{d}\cos\theta\,\mathrm{d}\phi}{\iint_{\theta,\phi}e^{\vec{\mu}\cdot\vec{E}_0/kT}\,\mathrm{d}\cos\theta\,\mathrm{d}\phi} \quad (3)$$

This is a function of a single parameter, $f = \mu E_0/kT$ and gives the well-known Langevin function ($L_n(f)$).

For the two-dimensional case, dipolar rotation is limited to a single plane containing the z-axis, the direction of the poling axis. The integral can be reduced to

$$\langle\cos^n\theta\rangle_{2D} = \frac{\int_{\theta=0}^{2\pi}\cos^n\theta\, e^{f\cos\theta}\,\mathrm{d}\theta}{\int_{\theta=0}^{2\pi}e^{f\cos\theta}\,\mathrm{d}\theta} \quad (4)$$

and may be written in terms of Bessel functions, $J_n(z)$.[41] The one-dimensional case is explained in the Supporting Information.

Higher order parameters ($\langle\cos^2\theta\rangle$,$\langle\cos^3\theta\rangle$) for the 2D and 3D cases can be found from the lower order parameters by differentiation according to

$$\langle\cos^n\theta\rangle_{MD} = \left(\frac{\mathrm{d}}{\mathrm{d}f} + \langle\cos^1\theta\rangle_{MD}\right)\langle\cos^{n-1}\theta\rangle_{MD} \quad (5)$$

where M stands for the dimensionality. The $n = 2$ and $n = 3$ order parameters are shown in Table 1 for both $M = 2$ and $M = 3$ dimensionalities.

The relationships among the various order parameters give insight into the dimensionality of the system. For example, in the low f regime, the first- and third-order parameters are related by $\langle\cos^3\theta\rangle_{MD} \approx (3/(M+2))\langle\cos^1\theta\rangle_{MD}$. Corresponding approximate relations for the 2D and 3D cases were derived numerically to give

$$\langle\cos^3\theta\rangle_{2D} \approx \sqrt{\frac{5}{4}\left(\langle P_2\rangle_{2D} - \frac{1}{4}\right)}\langle\cos^3\theta\rangle_{3D} \approx \sqrt{\frac{3}{5}\langle P_2\rangle_{3D}} \quad (6)$$

TABLE 1: Equations for Calculating Second- and Third-Degree Order Parameters for Two- and Three-Dimensional Systems[a]

$\langle\cos^n\theta\rangle$	2D order parameters	3D order parameters
$n=2$	$\langle\cos^2\theta\rangle_{2D} = \frac{1}{2}\left\{1 - \frac{J_2(-if)}{J_0(-if)}\right\}$	$\langle\cos^2\theta\rangle_{3D} = 1 - 2\frac{\langle\cos^1\theta\rangle_{3D}}{f}$
$n=3$	$\langle\cos^3\theta\rangle_{2D} = \frac{3}{4}\langle\cos^1\theta\rangle_{2D} + \frac{1}{4}\frac{-iJ_3(-if)}{J_0(-if)}$	$\langle\cos^3\theta\rangle_{3D} = \frac{2}{f}\left(3\frac{\langle\cos^1\theta\rangle_{3D}}{f} - 1\right) + \langle\cos^1\theta\rangle_{3D}$

[a] First-degree order parameters are given in the Supporting Information.

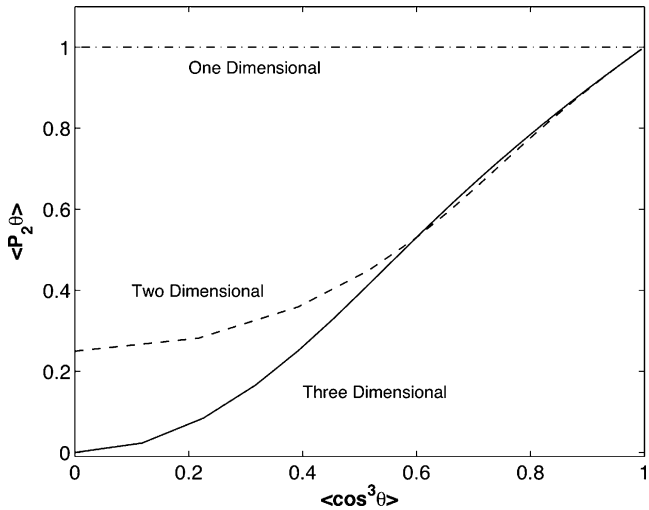

Figure 2. The different degrees of dimensionality are shown through the relationship of centrosymmetric order parameter versus acentric order parameter. The lowest curve corresponds to a system in which environmental restrictions are minimal, and the middle curve corresponds to a 2D system in which molecular rotation is confined to a plane. The upper curve corresponds to a one-dimensional lattice in which molecules exhibit perfect centrosymmetric order and may be only parallel or antiparallel to each other.

Here, $\langle P_2\rangle_{MD}$ is the centrosymmetric order parameter related to $\langle\cos^2\theta\rangle_{MD}$ through

$$\langle P_2\rangle_{MD} = \frac{3\langle\cos^2\theta\rangle_{MD} - 1}{2} \tag{7}$$

The expressions in eq 6 can be used to calculate $\langle\cos^3\theta\rangle$ from experimentally measured $\langle P_2\rangle$ values for perfectly two- and three-dimensional systems, respectively, assuming that the order is not too large so that the approximation provided by eq 6 is valid. However, a system might not be perfectly one-, two-, or three-dimensional, but may have an apparent fractional dimensionality. An approximate continuous interpolation between the 2D and 3D equations in the linear regime gives

$$\langle\cos^3\theta\rangle_{MD} \approx \sqrt{\left(\frac{9-2M}{2+M}\right)\left(\langle P_2\rangle_{MD} - \frac{3-M}{2M}\right)} \tag{8}$$

This is a convenient approximation relating $\langle\cos^3\theta\rangle$ to $\langle P_2\rangle$ that is accurate over a large range of f and for $2 \le M \le 3$ (Note: this approximation cannot be applied to the $M = 1$ case because $\langle P_2\rangle_{1D} = 1$, and is independent of f). Figure 2 illustrates how the $\langle P_2\rangle$-to-$\langle\cos^3\theta\rangle$ relationship changes with the dimensionality of the system. All three curves correspond to the independent particle limit, where the chromophore concentration is low enough that intermolecular interactions are negligible.

The dimensional restrictions imposed on the dipoles can represent external factors that reduce the dimensionality of free motion in practice. These factors can arise from environmental, steric, electrostatic, or any combination of such interactions. The three-dimensional curve in Figure 2 represents the type of order observed in a typical poled polymer system. The two-dimensional curve corresponds to a dipole restricted to free rotation in a plane. In practice, such a lattice might be created by other ordered dipoles (binary chromophore EO materials)[42,36,19,43] or by an ordered host matrix created by forces with alignment capability that are independent of the poling field. The dimensionality parameter M conveniently encapsulates the restricted orientation possibilities that chromophores experience as a result of the combined influences of poling field and intermolecular interactions. Using experimental results for $\langle P_2\rangle$ and r_{33}, $\langle\cos^3\theta\rangle$ can be obtained; M can then be evaluated quantitatively using eq 8. Even though the curves in Figure 2 are derived from independent particle limits and represent low chromophore concentration, it is demonstrated in the next section through computer simulation of order that the relation in eq 8 is still meaningful for dense systems.

Simulation of Reduced Dimensionality at High Concentration. To further investigate the relationship between acentric order, centrosymmetric order, and dimensionality, we have performed course-grained rigid body Monte Carlo (RBMC) computer modeling studies of strongly dipolar ellipsoids at high densities. We use the RBMC method, which has been shown to correlate well with experimental results to understand electric-field-induced acentric chromophore alignment.[22,23,1,20,21,44] From the simulations, any degree of order parameter, including $\langle\cos^1\theta\rangle$, $\langle\cos^2\theta\rangle$, and $\langle\cos^3\theta\rangle$, with respect to the poling axis can be calculated.

The model used here represents the chromophore core as a nonpolarizable rigid ellipsoid containing a single permanent dipole of strength μ aligned with the unique axis of the ellipsoid. These ellipsoids are parametrized as a coarse-grained approximation to the core of the F2 chromophore.[38] Protecting groups, side chains, and other functionalizations are neglected in the simple model used for these simulations. Simulations were run using self-consistent reaction field (SCRF) boundary conditions,[45−47] with dielectric effects from the medium represented by setting the background dielectric constant in the reaction field cavity[48] to $\varepsilon_\infty = n$.[2] Simulation parameters are shown in Table 2.

Here, σ_{LJ} and ε_{LJ} are the Lennard-Jones ellipsoidal lengths and interaction energy, respectively.[49] The σ_{LJ} were based on the molecular volume of the chromophore core, which was calculated along with the dipole moment using Spartan '08[50] at the B3LYP/6-31G* level of theory. The Lennard-Jones energy

TABLE 2: Rigid-Body Parameters

σ_{LJ} (Å)	ε_{LJ} (K)	μ (D)	molecular V (Å^3)	N (molecules/cc) (neat)
7.0 (x, y), 21.0 (z)	217.4	23.5	538.8	1.26×10^{21}

TABLE 3: Order Parameters and Dimensionalities for the Simulations Represented in Figure 3[a]

E_p (V/μm)	N^b	$\langle P_2 \rangle$	$\langle \cos^3 \theta \rangle$	$\langle \cos^3 \theta \rangle / \langle P_2 \rangle$	M
50	1.26	0.015 ± 0.001	0.052 ± 0.0001	3.5 ± 0.3	2.9
	2.52	0.017 ± 0.003	0.046 ± 0.0003	2.7 ± 0.4	2.9
	3.78	0.017 ± 0.003	0.040 ± 0.0002	2.3 ± 0.4	2.9
	5.04[c]	0.042 ± 0.007	0.035 ± 0.0003	0.8 ± 0.1	2.8
	6.30[c]	0.42 ± 0.11	0.013 ± 0.001	0.03 ± 0.01	<2
75	1.26	0.033 ± 0.001	0.082 ± 0.0003	2.4 ± 0.1	2.9
	2.52	0.035 ± 0.002	0.073 ± 0.0004	2.1 ± 0.1	2.8
	3.78	0.048 ± 0.002	0.066 ± 0.0006	1.4 ± 0.1	2.8
	5.04[c]	0.073 ± 0.005	0.057 ± 0.0007	0.8 ± 0.1	2.6
	6.30[c]	0.76 ± 0.11	0.022 ± 0.002	0.03 ± 0.005	<2

[a] $T = 382$ K, $m = 1728$ particles. [b] ($\times 10^{20}$ molecules/cc). [c] Longer runs were required for convergence at these densities.

used is typical of small organic molecules.[47,51] The N given in Table 2 represents the hypothetical number density of a pure solid of the chromophore core in C1.

All simulations were run at 382 K (the actual poling temperature) using the refractive index of solid PMMA ($n = 1.5$), giving a background dielectric constant $\varepsilon_\infty = 2.25$. Simulations were run at molecular densities ranging from 1.26×10^{20} molecules/cc to 6.3×10^{20} molecules/cc, and at two external field strengths (50 and 75 V/μm). The field strength was defined as the macroscopic field, E_p, and dynamically corrected by the dielectric behavior of the system using a modified Onsager cavity field to calculate E_0.[41] All simulations contained 1728 particles (m). Simulations at the lowest three densities were run for 40,000 total MC cycles, with 1728 steps per cycle for a total of 6.9×10^7 configurations. The first 1000 cycles were run without electrostatics to break up the initial lattice, and the expectation values of the acentric order parameter, $\langle \cos^3 \theta \rangle$, and centrosymmetric order parameter, $\langle P_2 \rangle$, were calculated from the last 20,000 MC cycles. Simulations at the highest densities required longer run lengths to achieve convergence.[41] Because both order parameters were calculated directly, the effective dimensionality of simulations can be obtained using eq 8. Final averages and errors were obtained from five replicates of each simulation using different random number seeds. The results are depicted in Figure 3 and summarized in Table 3.

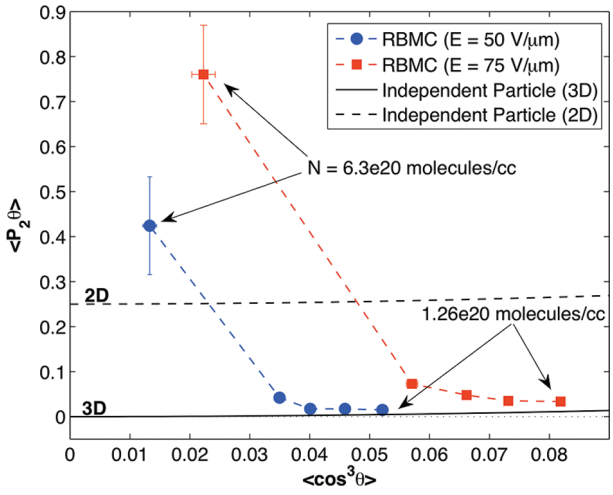

Figure 3. The dimensionalities of the simulations performed at different densities are shown and overlaid with the theoretical curves derived from the independent particle limit previously given in Figure 2. The blue data are simulations poled at 50 V/μm; the red data are simulations poled at 75 V/μm. Larger values of $\langle \cos^3 \theta \rangle$ are observed for the higher simulated poling field. The highest-density RBMC data also exhibits reduced dimensionality ($M < 2$) due to a very large $\langle P_2 \rangle$ value.

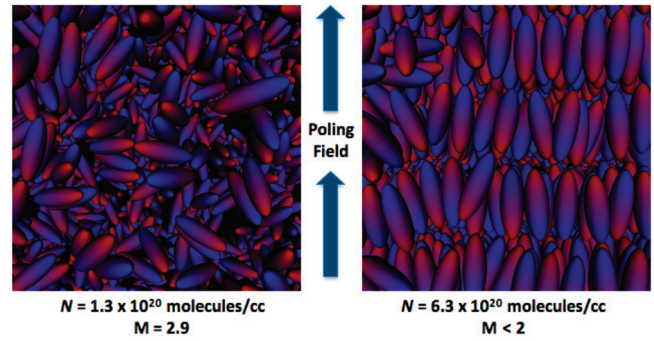

Figure 4. Images of ensembles of poled dipolar ellipsoids created from the RBMC simulation.[52] Two different densities are shown, poled at $E_p = 50$ V/μm. The left image, corresponding to a system with low N, exhibits low centrosymmetric order and is nearly 3D. The image on the right, corresponding to a higher-number-density system, exhibits high centrosymmetric order along the poling field axis and is less than 2-dimensional.

Table 3 illustrates that $\langle \cos^3 \theta \rangle$ monotonically decreases with increasing number density for dipolar ellipsoids, consistent with previous literature.[21−23] However, $\langle P_2 \rangle$, calculated directly from $\langle \cos^2 \theta \rangle$, slowly increases with number density up to 5.04×10^{20} molecules/cc chromophore density. Reduction of the ratio of the order parameters ($\langle \cos^3 \theta \rangle / \langle P_2 \rangle$) implies reduced dimensionality. Figure 3 demonstrates that the dimensionality of the system remains nearly 3D at the lower three densities, particularly at the lower poling field strength. Further increases in ellipsoid density higher than 5.04×10^{20} molecules/cc result in an abrupt increase in $\langle P_2 \rangle$, as demonstrated in Figure 4. The orientation of the director axis for the ordered phase is defined by the direction of the poling field.

Figure 4 suggests that a disorder−order transition occurs under poling conditions when the ellipsoid density becomes sufficiently high. A similar transition was observed in fully atomistic models of chromophores simulated by Hayden and co-workers.[53] This apparent phase transition appears to be responsible for the abrupt increase in $\langle P_2 \rangle$ and in the decrease of the $\langle \cos^3 \theta \rangle / \langle P_2 \rangle$ ratio, indicating a lower than two-dimensional system. In these simulations, the change in the $\langle \cos^3 \theta \rangle / \langle P_2 \rangle$ ratio comes from both the decrease in $\langle \cos^3 \theta \rangle$ and the increase in $\langle P_2 \rangle$. To confirm these results, control simulations with zero dipole moments under an applied poling field and, separately, simulations with strong dipoles under no poling field were performed. No phase transition occurred when the molecules had zero dipole moments, but in simulations with strong dipoles present in the absence of a poling field, a phase transition toward centrosymmetric order along a random director axis occurred. The results from these simulations suggest that the poling field assists in establishing a director axis for the formation of the ordered phase.

TABLE 4: Experimental Data Used to Estimate the Dimensionality (*M*) of C1, F2 in PMMA, and P3

material	r_{33}/E_p[a]	N[b]	r_{33}/NE_p[c]	$\langle P_2\rangle$[d]	$\beta_{zzz}(-\omega; 0, \omega)$[e]	$g(\omega)/n^4$	$\langle\cos^3\theta\rangle$[f]	$N\langle\cos^3\theta\rangle$	M
C1 (TiO_2)	1.92 ± 0.04	4.4	0.28	0.19 ± 0.015	3000 ± 300	0.57	0.15 ± 0.02	0.66 ± 0.07	2.2
F2/PMMA	0.45 ± 0.02	1.7	0.26	0.035 ± 0.01	3500 ± 600	0.62	0.073 ± 0.01	0.12 ± 0.02	2.8
F2/PMMA[g]	0.15 ± 0.02	3.6	0.042	0.04 ± 0.02	3500 ± 600	0.57	0.015 ± 0.003	0.054 ± 0.01	2.8
P3[h]	1.42 ± 0.04	6.4	0.22	0.019 ± 0.005	4033[i] ± 126	0.52	0.063 ± 0.003	0.41 ± 0.02	2.9

[a] In $(nm/V)^2$. [b] $\times 10^{20}$ molecules/cc. [c] In $(nm/V)^2$(cc/10^{20} molecules). [d] $\langle P_2\rangle$ at $E_p = 50$ V/μm for C1, F2/PMMA (low density), and P3; $E_p = 60$ V/μm for F2/PMMA (high density). [e] Units $= (\times 10^{-30}$ esu); measured experimentally using HRS. [f] Estimated from eq 10 using r_{33}/E_p ($E_p = 50$ V/μm), except for F2/PMMA at high density where $E_p = 60$ V/μm. [g] $E_p = 60$ V/μm for F2/PMMA at high density. [h] P3 (i.e., PSLD-33) data was previously reported.[44] [i] Theoretical value calculated using TD-DFT.[13,44]

Materials and Methods

The molecular structures of C1 and F2 are shown in Figure 1. The synthesis of C1 is relatively straightforward, accomplished through modification of known methods, and will be presented in detail elsewhere. The synthesis of F2 is reported elsewhere.[38] The synthesis and characterization for P3, an electro-optic multichromophore-containing dendrimer (EOMD) material previously referred to as PSLD-33, is reported elsewhere.[20] Thin films of both C1 (neat, $N = 4.4 \times 10^{20}$ molecules/cc) and F2 (20 wt %; $N = 1.7 \times 10^{20}$ molecules/cc) in PMMA (purchased from Sigma Aldrich and purified[20]) were produced by spin-casting solutions of 8−9 wt % total solids in 1,1,2-trichloroethane onto indium tin oxide (ITO)-coated substrates to give thin films of ~1 μm thickness. For absorption spectroscopy experiments of C1, a 90 nm layer of titanium dioxide (TiO_2/titania) was applied to the ITO substrates using a sol−gel method prior to applying the EO layer.[1,54] Samples of C1 on bare ITO were limited to poling voltages of 40 V/μm due to high conductivity; samples approaching this limit were subject to potential damage, complicating analysis. TiO_2 was applied as a charge-blocking layer to allow improved poling conditions and sample consistency. The thickness of the TiO_2 layer constitutes <10% of the total material thickness coated onto the ITO/glass substrate, causing negligible change in the applied poling field across the sample[41] and improved poling efficiency for C1 ($r_{33}/E_p = 1.9$ $(nm/V)^2$).

Thin films of C1 and F2/PMMA were annealed at 55 and 65 °C, respectively, under vacuum for 24 h to remove residual solvent. Gold electrodes were then deposited on top of the films by sputter-coating from argon plasma. Several samples of both materials were poled ~3 °C below the T_g (~80 °C for C1 and 115 °C for F2 in PMMA)[30] under optimized conditions using increasing values of applied poling field. Poling-induced r_{33} values were determined for all materials using an attenuated total reflection (ATR) apparatus ($\lambda_{ex\text{-}p}(ATR) = 1310$ nm) after the external poling field was removed. Linear regression of plots of r_{33} vs E_p yielded the respective values of poling efficiency for each material. The ATR technique was chosen for r_{33} measurement because it does not suffer from the potential experimental error associated with the common fixed angle reflection mode ellipsometry (Teng-Man) technique when operated at telecommunications wavelengths.[55]

To investigate poling-induced order and dimensionality, poled samples of both C1 and F2/PMMA were evaluated using variable angle polarization referenced absorption spectroscopy (VAPRAS) to determine the centrosymmetric order parameter, $\langle P_2\rangle$.[1,56] To evaluate $\langle\cos^3\theta\rangle$ using eq 1, all required parameters were evaluated experimentally.[44] The molecular first-order hyperpolarizabilities ($\beta_{HRS}(-2\omega; \omega, \omega)$) of both C1 and F2 in chloroform were evaluated using hyper-Rayleigh scattering (HRS, $\lambda_{HRS} = 1907$ nm).[1,44,57−59] To estimate local field factors affecting both spin-cast materials,[40,44] variable angle spectroscopic ellipsometry (VASE) measurements were performed to obtain the real and imaginary contributions to the complex refractive index of C1 and F2/PMMA films in the wavelength range of $\lambda_{VASE} = 300-1700$ nm.[44,60]

Results and Discussion

The poling-induced optical properties, centrosymmetric, and acentric order of the C1 material, a monolithic pendant-modified organic glass possessing a chromophore mass fraction of 41.7% ($N = 4.4 \times 10^{20}$ molecules/cc), are compared with a conventional guest−host material consisting of the highly dipolar chromophore F2 doped into PMMA polymer at 20% ($N = 1.7 \times 10^{20}$ molecules/cc) (Figure 1).[38] This concentration of F2 in PMMA represents the optimized loading level.[1]

The coumarin pendant groups were introduced in the design of C1 (Figure 1) because this type of moiety is known to form liquid crystalline phases in neat films and in various examples of side-chain polymers.[61−63] Our objective was to use the intercoumarin interactions that govern ordered phase formation to introduce spatially anisotropic interactions to the electro-optic chromophores. These interactions are "soft" at relatively low temperatures, enabling them to be melted and reformed easily. The labile nature of these interactions facilitates poling and annealing under strong electric fields.

The F2 chromophore/PMMA host system was chosen for comparison because the chromophore core is the same as in C1. For further evaluation, C1 can be compared with P3 (previously reported as PSLD-33),[20] an electro-optic multichromophore containing dendrimer (EOMD) material with high chromophore concentration ($N = 6.4 \times 10^{20}$ molecules/cc) containing the same chromophore core as in C1. EOMD materials were designed with only the concept of site isolation in mind, unlike C1, which incorporates directed interactions.[20,30,44] Computer modeling results and experimental analyses have suggested that an enhancement in $N\langle\cos^3\theta\rangle$ in EOMD materials was obtained through site isolation by driving N to high levels; however, a severe trade-off between N and $\langle\cos^3\theta\rangle/E_p$ has been shown to exist in EOMD materials.[20,44] The structure of P3 is reported elsewhere.[20,41]

Drawing comparisons between monolithic organic EO materials and more traditional chromophore guest/polymer host composite materials is complicated by a number of factors, including differences in $\beta_{zzz}(-\omega; 0, \omega)$ due to changes in the dielectric properties of the host material.[15,17,20,44,64,65,14,66] However, when these effects are accounted for, comparisons between materials on the basis of poling efficiency, r_{33}/E_p (EO activity achieved for a given poling field strength), are useful for evaluating poling induced order. Poling efficiencies for C1, F2/PMMA, and P3 are given in Table 4.

Upon poling and ATR analysis, samples of C1 ($N = 4.4 \times 10^{20}$ molecules/cc) on ITO substrates were found to have nearly

three times the poling efficiency of samples of free chromophore F2 loaded at $N = 1.7 \times 10^{20}$ molecules/cc into PMMA host on ITO substrates. From these poling efficiencies, C1 displays nearly the same r_{33}/NE_p, implying that $\beta_{zzz}(\omega, \varepsilon)\cdot\langle\cos^3\theta\rangle/E_p$ is nearly the same in both materials, despite a significant (3-fold) increase in chromophore number density in the C1 material (eq 9).

$$\frac{r_{33}}{E_p} = N\beta_{zzz}(\omega, \varepsilon)\left\{\frac{\langle\cos^3\theta\rangle}{E_p}\right\}\frac{2g(\omega)}{n_\omega^4} \qquad (9)$$

The combination of VAPRAS, HRS, and VASE experiments and measurements of r_{33}/E_p allows access to the relationship between the order parameters $\langle P_2\rangle$ and $\langle\cos^3\theta\rangle$. Currently, no direct method is known to independently measure $\langle\cos^3\theta\rangle$. However, in a material that contains chromophores and possesses directional anisotropy, the $\langle P_2\rangle$ parameter can be evaluated using a number of absorption spectroscopy methods. The normal incidence method (NIM) is the simplest of these methods.[67,68,36,69] Samples of C1 on TiO_2-coated substrates[1] were poled and measured by NIM. To obtain a complementary and more thorough measurement, the VAPRAS method[56] was used to measure $\langle P_2\rangle$ for the majority of the comparative materials. VAPRAS has been used to measure poling-induced order in several materials and correlated with Monte Carlo statistical mechanical modeling to estimate $\langle\cos^3\theta\rangle$.[1,44] VAPRAS analysis was performed on C1 on TiO_2-coated substrates and F2 in PMMA. All $\langle P_2\rangle$ values are presented in Table 5.

TABLE 5: Experimental $\langle P_2\rangle$ Values Determined Using NIM or VAPRAS for C1, F2/PMMA, and P3

material	N^a	$E_p{}^b$	$r_{33}{}^c$	$\langle P_2\rangle_{NIM}$	$\langle P_2\rangle_{VAPRAS}$
C1	4.4	40	76	0.16 ± 0.04	0.13 ± 0.01
		50	95		0.19 ± 0.015
F2/PMMA	1.7	50	22		0.03 ± 0.01
		75	32		0.065 ± 0.019
	3.6	60	9	0.04 ± 0.02	
P3	6.5	50	71		0.019 ± 0.005^d

[a] $\times 10^{20}$ molecules/cc. [b] In V/μm. [c] In pm/V. [d] Previously reported.[20]

Both NIM and VAPRAS data are in close agreement for the C1 material. For comparison, VAPRAS was performed on samples of F2 in PMMA loaded at $N = 1.7 \times 10^{20}$, the optimal number density for this system. At the same applied poling voltage, $\langle P_2\rangle_{VAPRAS}$ for C1 is 6 times higher than $\langle P_2\rangle_{VAPRAS}$ for F2. As an additional comparison, NIM was performed on samples of F2 in PMMA loaded at high chromophore concentration ($N = 3.6 \times 10^{20}$), similar to C1. High-concentration samples of F2 in PMMA yielded almost the same $\langle P_2\rangle$ value as the optimal concentration, but with severely reduced r_{33}. The $\langle P_2\rangle$ value for C1 is a full order of magnitude higher than the P3 dendrimer (Table 5). These experimental $\langle P_2\rangle$ values presented for all materials can be used to evaluate $\langle\cos^3\theta\rangle$ and quantify the dimensionality, M.

Experimental measurements of linear and nonlinear optical properties can be used to evaluate parameters in eq 1 and calculate $\langle\cos^3\theta\rangle$.[44] Using $\beta_{HRS}(-2\omega; \omega, \omega)$, values for both C1 and F2 in chloroform solution with rotational averaging appropriate for hyper-Rayleigh scattering[70−72] together with the two-state model frequency dependence ($\lambda_{HRS} = 1907$ nm and $\lambda_{ATR} = 1310$ nm) enables one to interconvert frequency dependences and fix the relation between $\beta_{HRS}(-2\omega; \omega, \omega)$ and $\beta_{zzz}(\omega, \varepsilon)$. Corrections for differences in dielectric effects as previously described[44] were applied, yielding $\beta_{zzz}(-\omega; 0, \omega)$ values for F2 and C1 ($3500 \pm 600 \times 10^{-30}$ esu and $3000 \pm 300 \times 10^{-30}$ esu, respectively). To evaluate the $g(\omega)/n^4$ term (Lorentz−Onsager local field factors) used in eq 1, refractive index data were obtained for both F2 and C1 using VASE (Figure 5).[60,73,44]

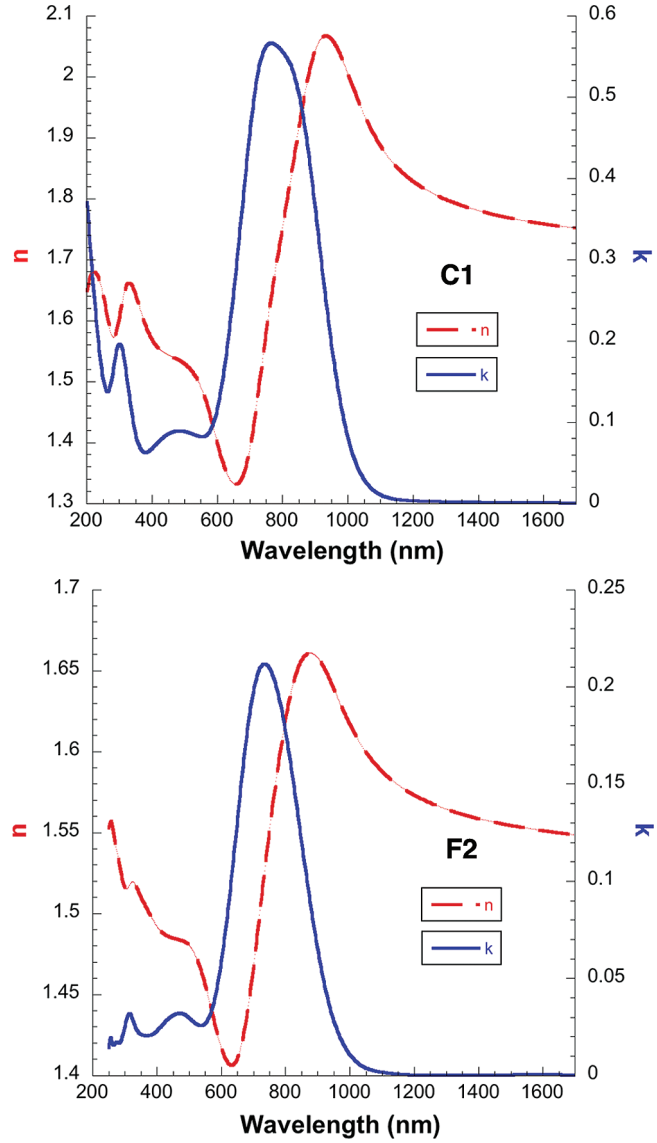

Figure 5. VASE analysis of the real (n, red line) and imaginary (k, blue line) refractive index components vs wavelength are shown. Top: C1, $n\{1700\text{ nm}\} = 1.75$, $n_\omega\{1310\text{ nm}\} = 1.8$. Bottom: 1×10^{20} molecules/cc F2 in PMMA; $n\{1700\text{ nm}\} = 1.55$, $n_\omega\{1310\text{ nm}\} = 1.56$. Here, n is the refractive index (long wavelength limit) approximated by the real part at $\lambda = 1700$ nm, and η_ω is the refractive index at the r_{33} measurement wavelength $\lambda = 1310$ nm.

We can calculate $g(\omega)/n^4$ from $g(\omega) = f_l^0\,(f_l^\omega)^2$ using $f_l^0 = \varepsilon(n^2 + 2)/(n^2 + 2\varepsilon)$ and $f_l^\omega = (n_\omega{}^2 + 2)/3$. The low-frequency dielectric constant, ε, was measured using standard capacitance methods[44] and estimated as $\varepsilon = 4.0$ for 1.7×10^{20} molecules/cc F2 in PMMA and $\varepsilon = 5.3$ for C1. Using these data, we find that $g(\omega)/n_\omega{}^4 = 0.62$ for F2 in PMMA and $g(\omega)/n_\omega{}^4 = 0.57$ for C1. Values for $\beta_{zzz}(-\omega; 0, \omega)$, r_{33}/E_p, and $g(\omega)/n_\omega{}^4$ with

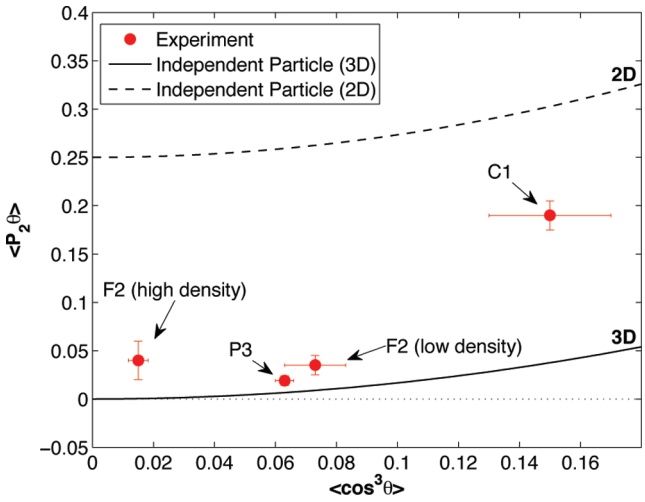

Figure 6. Experimental data overlaid with predicted 2D and 3D dimensionality curves derived from the independent particle limit as presented earlier in Figure 2. C1 is nearly two-dimensional, exhibiting reduced dimensionality due to its high degree of centrosymmetric order as compared with its degree of acentric order. F2 in PMMA (high and low density) and P3 are approximately three-dimensional, exhibiting much lower $\langle P_2 \rangle$ and $\langle \cos^3 \theta \rangle$ values.

consistent units are summarized in Table 4 and can be used to obtain $\langle \cos^3 \theta \rangle$ from eq 10, a rearrangement of eq 1 or 9.

$$\frac{\langle \cos^3 \theta \rangle}{E_p} = 0.5\left\{\frac{r_{33}}{E_p}\right\}/N \cdot \beta_{zzz}(-\omega;0,\omega) \cdot \left(\frac{g(\omega)}{n_\omega{}^4}\right) \qquad (10)$$

Using eq 10, $\langle \cos^3 \theta \rangle$ values for all materials are presented in Table 4. These data illustrate that the relationships between $\langle P_2 \rangle$ and $\langle \cos^3 \theta \rangle$ are different for guest/host F2 in PMMA and the pendant modified organic glass, C1. The $\langle P_2 \rangle$ value for C1 is over 5 times higher than that of optimally loaded F2 in PMMA, whereas the $\langle \cos^3 \theta \rangle$ value for C1 is 2 times higher. Furthermore, $\langle \cos^3 \theta \rangle$ for C1 is a full order of magnitude higher than $\langle \cos^3 \theta \rangle$ for F2 loaded into PMMA at high number density (similar to that of C1) and P3, illustrating a sharp decrease in $\langle \cos^3 \theta \rangle$ with increasing N for the poled polymer system and a material system shown to demonstrate site isolation. This trend has been confirmed by theoretical Monte Carlo statistical mechanical modeling.[21,22] However $\langle \cos^3 \theta \rangle / E_p$ is increased in the C1 material, illustrating that the loading parameter, $N\langle \cos^3 \theta \rangle$, is over 5 times higher for C1 than F2 (Table 4).

Equation 8 may be used to quantify the dimensionality of the poled solid-state materials C1, F2 in PMMA, and P3 based on these estimates of $\langle \cos^3 \theta \rangle$ and $\langle P_2 \rangle$ values. Dimensionalities for these systems were calculated to be $M \approx 2.8$ for F2 in PMMA and $M \approx 2.2$ for C1, confirming the hypothesis that dimensional restriction occurs in the case of C1. Furthermore, eq 8 yields $M \approx 2.9$ for the P3 dendrimer, demonstrating a lack of reduced dimensionality in the EOMD system consisting of the same F2 chromophore, but without coumarin pendant groups. Figure 6 compares the values of C1, F2/PMMA, and P3 and the general descriptions of dimensionality.

The large $\langle P_2 \rangle$ for C1 compared to its $\langle \cos^3 \theta \rangle$ value signifies reduced dimensionality, with the increase in $\langle P_2 \rangle$ being sufficiently large to shift the ratio of the order parameters, even with an increase in $\langle \cos^3 \theta \rangle$. We propose that this reduced dimensionality is achieved in part by the formation of some degree of secondary (matrix) order that originates from intercoumarin interactions directed by the poling field and chromophore reorientation. Even though liquid crystalline phases are not formed in the case of C1,[41] the intercoumarin interactions may still act to create interaction potentials that influence the poling-induced acentric order.

Conclusions

A dipolar EO chromophore core was functionalized with two identical coumarin pendant groups to introduce interpendant directed interactions. These interactions create a noncovalently associated glassy matrix that helps restrict poling-induced chromophore reorientation, equivalent to reducing the effective dimensionality of the system. By comparing the poling efficiency of C1 and the analogous free chromophore core F2 loaded at its optimum concentration into an inert host, it was found that even though chromophore number density increased almost 3-fold in C1, the ordering efficiency, $\langle \cos^3 \theta \rangle / E_p$, was not compromised and was even enhanced. Even though $\langle \cos^3 \theta \rangle$ is similar in both poled materials (within a factor of 2), $\langle P_2 \rangle$ was found to be 5-fold larger in the C1 samples. This difference corresponds to a change from what is effectively a 3D matrix (F2 in PMMA) to an almost 2D matrix (C1), illustrating that the relationship between $\langle P_2 \rangle$ and $\langle \cos^3 \theta \rangle$ can be reasonably well understood in terms of a reduced dimensionality.

Furthermore, previously reported EOMD materials composed of high densities of a chromophore core similar to that in C1 do not exhibit a reduction in dimensionality, with $M \approx 3$. Even though $N\langle \cos^3 \theta \rangle$ was effectively enhanced by utilizing shape effects to promote chromophore−chromophore isolation in EO dendrimers, $\langle \cos^3 \theta \rangle / E_p$ was still lower than for a guest/host material at optimum loading.[20,44] In contrast, specifically designed spatially anisotropic interchromophore interactions in C1 exemplify the following gains in EO materials design: a higher $\langle \cos^3 \theta \rangle / E_p$ than an optimized guest/host, despite higher N; poling efficiencies higher than those seen in the dendrimers, even though N is reduced in C1; and a significantly enhanced loading parameter, $N\langle \cos^3 \theta \rangle$.

More detailed theoretical studies are currently underway to explore C1 and modifications thereof. Additional studies of the thermal behavior and optical characteristics of C1 are in progress to determine the energetics of interpendant interactions vs interchromophore electrostatics as well as the relative orientations of the pendant-groups and chromophore core.

Acknowledgment. The National Science Foundation (DMR-0905686, DMR-0120967), the Air Force Office of Scientific Research (FA9550-09-1-0589 MOD), and the IC/National Geospatial Intelligence Agency (HM1582-09-1-0026) are acknowledged for funding. Dr. Jianing Sun and James N. Hilfiker of J. A. Woollam Inc. in Lincoln, NE are gratefully acknowledged for the variable angle spectroscopic (VASE) measurements. Dr. Arumugasamy Elangovan is thanked for helpful discussions. Benjamin H. Sibelman is thanked for developing a visualizer for our simulations.

Supporting Information Available: Detailed explanation of the characterization and simulation methods and further derivation of the Reduced Dimensionality Theory. This material is available free of charge via the Internet at http://pubs.acs.org.

References and Notes

(1) Dalton, L. R.; Sullivan, P. A.; Bale, D. H. *Chem. Rev.* **2010**, *110*, 25.

(2) Zyss, J. *Molecular Nonlinear Optics*; Academic: New York, 1994.

(3) Kuzyk, M. G.; Dirk, C. W. *Characterization Techniques and Tabulations for Organic Nonlinear Optical Materials*; Marcel Dekkar: New York, NY, 1998.

(4) Nalwa, H. S.; Miyata, S. *Nonlinear Optics of Organic Molecules and Polymers*; CRC Press: Boca Raton, 1997.

(5) Raimundo, J.-M.; Blanchard, P.; Gallego-Planas, N.; Mercier, N.; Ledoux-Rak, I.; Hierle, R.; Roncali, J. *J. Org. Chem.* **2002**, *67*, 205.

(6) Raimundo, J.-M.; Blanchard, P.; Michaux, L.; Roncali, J.; Ledoux-Rak, I.; Hierle, R. *Chem. Commun.* **2000**, *17*, 1597.

(7) Robinson, B. H.; Dalton, L. R.; Harper, A. W.; Ren, A.; Wang, F.; Zhang, C.; Todorova, G.; Lee, M.; Aniszfeld, R.; Garner, S.; Chen, A.; Steier, W. H.; Houbrecht, S.; Persoons, A.; Ledoux, I.; Zyss, J.; Jen, A. K. Y. *Chem. Phys.* **1999**, *245*, 35–50.

(8) Kanis, D. R.; Ratner, M. A.; Marks, T. J. *Chem. Rev.* **1994**, *94*, 195.

(9) Marder, S. R.; Perry, J. W.; Bourhill, G.; Gorman, C. B.; Tiemann, B. G.; Mansour, K. *Science* **1993**, *261*, 186.

(10) Marder, S. R.; Gorman, C. B.; Meyers, F.; Perry, J. W.; Bourhil, G.; Bredas, J. L.; Pierce, B. M. *Science* **1994**, *265*, 632.

(11) Kuzyk, M. G. *Phys. Rev. A* **2005**, *72*, 053819.

(12) Albert, I. D. L.; Marks, T. J.; Ratner, M. A. *J. Am. Chem. Soc.* **1997**, *119*, 6575.

(13) Isborn, C. M.; Leclercq, A.; Vila, F. D.; Dalton, L. R.; Bre'das, J. L.; Eichinger, B. E.; Robinson, B. H. *J. Phys. Chem. A* **2007**, *111*, 1319.

(14) Takimoto, Y.; Isborn, C. M.; Eichinger, B. E.; Rehr, J. J.; Robinson, B. H. *J. Phys. Chem. C* **2008**, *112*, 8016.

(15) Kinnibrugh, T.; Bhattacharjee, S.; Sullivan, P.; Isborn, C.; Robinson, B. H.; Eichinger, B. E. *J. Phys. Chem. B* **2006**, *110*, 13512.

(16) Chafin, A. P.; Lindsay, G. A. *J. Phys Chem. C* **2008**, *112*, 7829.

(17) Bourhill, G.; Bredas, J. L.; Cheng, L.-T.; Marder, S. R.; Meyers, F.; Perry, J. W.; Tiemann, B. G. *J. Am. Chem. Soc.* **1994**, *116*, 2619.

(18) Davies, J. A.; Elangovan, A.; Sullivan, P. A.; Olbricht, B. C.; Bale, D. H.; Ewy, T. R.; Isborn, C. M.; Eichinger, B. E.; Robinson, B. H.; Reid, P. J.; Li, X.; Dalton, L. R. *J. Am. Chem. Soc.* **2008**, *130*, 10565.

(19) Kim, T.-D.; Luo, J.; Cheng, Y.-J.; Shi, Z.; Hau, S.; Jang, S.-H.; Zhou, X. H.; Tian, Y.; Polishak, B.; Huang, S.; Ma, H.; Dalton, L. R.; Jen, A. K.-Y. *J. Phys. Chem. C* **2008**, *112*, 8091.

(20) Sullivan, P. A.; Rommel, H.; Liao, Y.; Olbricht, B. C.; Akelaitis, A. J. P.; Firestone, K. A.; Kang, J.-W.; Luo, J.; Choi, D. H.; Eichinger, B. E.; Reid, P.; Chen, A.; Robinson, B. H.; Dalton, L. R. *J. Am. Chem. Soc.* **2007**, *129*, 7523.

(21) Rommel, H. L.; Robinson, B. H. *J. Phys. Chem. C* **2007**, *111*, 18765.

(22) Robinson, B. H.; Dalton, L. R. *J. Phys. Chem. A* **2000**, *104*, 4785.

(23) Nielsen, R. D.; Rommel, H. L.; Robinson, B. H. *J. Phys. Chem. B* **2004**, *108*, 8659.

(24) Luo, J.; Haller, M.; Li, H.; Tang, H.-Z.; Jen, A. K.-Y.; Jakka, K.; Chou, C.-H.; Shu, C.-F. *Macromolecules* **2004**, *37*, 248.

(25) Luo, J.; Haller, M.; Ma, H.; Liu, S.; Kim, T.-D.; Tian, Y.; Chen, B.; Jang, S.-H.; Dalton, L. R.; Jen, A. K.-Y. *J. Phys Chem. B* **2004**, *108*, 8523.

(26) Hammond, S. R.; Clot, O.; Firestone, K. A.; Bale, D. H.; Lao, D.; Haller, M.; Phelan, G. D.; Carlson, B.; Jen, A. K. Y.; Reid, P. J.; Dalton, L. R. *Chem. Mater.* **2008**, *20*, 3425.

(27) Ma, H.; Chen, B.; Sassa, T.; Dalton, L. R.; Jen, A. K.-Y. *J. Am. Chem. Soc.* **2001**, *123*, 986.

(28) Gopalan, P.; Katz, H. E.; McGee, D. J.; Erben, C.; Zielinski, T.; Bousquet, D.; Muller, D.; Grazul, J.; Olsson, Y. *J. Am. Chem. Soc.* **2004**, *126*, 1741.

(29) Do, J. Y.; Ju, J. J. *Macromol. Chem. Phys.* **2005**, 1326.

(30) Sullivan, P. A.; Akelaitis, A. J. P.; Lee, S. K.; McGrew, G.; Lee, S.; Choi, D. H.; Dalton, L. R. *Chem. Mater.* **2006**, *18*, 344.

(31) Bai, Y.; Song, N.; Gao, J. P.; Sun, X.; Wang, X.; Yu, G.; Wang, Z. Y. *J. Am. Chem. Soc.* **2005**, *127*, 2060.

(32) Zhu, Z.; Li, Z.; Tan, Y.; Li, Z.; Li, Q.; Zeng, Q.; Ye, C.; Qin, J. *Polymer* **2006**, *47*, 7881.

(33) Li, Z.; Qin, A.; Lam, J. W. Y.; Dong, Y.; Dong, Y.; Ye, C.; Williams, I. D.; Tang, Z. *Macromolecules* **2006**, *39*, 1436.

(34) Luo, J.; Liu, S.; Haller, M.; Liu, L.; Ma, H.; Jen, A. K.-Y. *Adv. Mater.* **2002**, *14*, 1763.

(35) Luo, J.; Ma, H.; Haller, M.; Jen, A. K.-Y.; Barto, R. R. *Chem. Commun.* **2002**, 888.

(36) Kim, T.-D.; Kang, J.-W.; Luo, J.; Jang, S.-H.; Ka, J.-W.; Tucker, N. M.; Benedict, J. B.; Dalton, L. R.; Gray, T.; Overney, R. M.; Park, D. H.; Herman, W. N.; Jen, A. K.-Y. *J. Am. Chem. Soc.* **2007**, *129*, 488.

(37) Olbricht, B. C.; Sullivan, P. A.; Wen, G.-A.; Mistry, A.; Davies, J. A.; Ewy, T. R.; Eichinger, B. E.; Robinson, B. H.; Reid, P. J.; Dalton, L. R. *J. Phys. Chem. C* **2008**, *112*, 7983.

(38) Liao, Y.; Anderson, C. A.; Sullivan, P. A.; Akelaitis, A. J. P.; Robinson, B. H.; Dalton, L. R. *Chem. Mater.* **2006**, *18*, 1062.

(39) Onsager, L. *J. Am. Chem. Soc.* **1936**, *58*, 1486.

(40) Singer, K. D.; Kuzyk, M. G.; Sohn, J. E. *J. Opt. Soc. Am. B* **1987**, *4*, 968.

(41) See the Supporting Information.

(42) Pereverzev, Y. V.; Gunnerson, K. N.; Prezhdo, O. V.; Sullivan, P. A.; Liao, Y.; Olbricht, B. C.; Akelaitis, A. J. P.; Jen, A. K. Y.; Dalton, L. R. *J. Phys. Chem. C* **2008**, *112*, 4355.

(43) Kim, T.-D.; Luo, J.; Ka, J.-W.; Hau, S.; Tian, Y.; Shi, Z.; Tucker, N. M.; Jang, S.-H.; Kang, J.-W.; Jen, A. K. Y. *Adv. Mater.* **2006**, *18*, 3038.

(44) Sullivan, P. A.; Rommel, H. L.; Takimoto, Y.; Hammond, S. R.; Bale, D. H.; Olbricht, B. C.; Liao, Y.; Rehr, J.; Eichinger, B. E.; Jen, A. K.-Y.; Reid, P. J.; Dalton, L. R.; Robinson, B. H. *J. Phys. Chem. B* **2009**, *113*, 15581.

(45) Barker, J. A.; Watts, R. O. *Mol. Phys.* **1973**, *26*, 789.

(46) Bartke, J.; Hentschke, R. *Mol. Phys.* **2006**, *104*, 3057.

(47) Leach, A. R. *Molecular Modeling: Principles and Applications*, 2nd ed.; Pearson Education: Harlow (UK), 2001.

(48) March, N. H.; Tosi, M. P. *Atomic Dynamics in Liquids*; Dover Publications, Inc.: New York, NY, 1976.

(49) Allen, M. P.; Tildesley, D. J. *Computer Simulations of Liquids.*; Clarendon: Oxford (UK), 1987.

(50) *Spartan '08*, 1.2.0 ed.; Wavefunction, Inc.: Irvine, CA, 2008.

(51) McQuarrie, D. A. *Statistical Mechanics*; University Science Books: Sausalito, CA, 2000.

(52) Sibelman, B. H. *Dipole X3D Translator*; 2.0 ed.; http://courses-.washington.edu/bhrchem/visualizer.php, 2009.

(53) Leahy-Hoppa, M. R.; Cunningham, P. D.; French, J. A.; Hayden, L. M. *J. Phys. Chem. A* **2006**, *110*, 5792.

(54) Alam, M. J.; Cameron, D. C. *J. Sol-Gel Sci. Technol.* **2002**, *25*, 137.

(55) Park, D. H.; Lee, C. H.; Herman, W. N. *Opt. Express* **2006**, *14*, 8866.

(56) Sullivan, P.; Dalton, L. R. *Acc. Chem. Res.* **2009**, online August 7; http://pubs.acs.org, doi: 10.1021/ar800264w.

(57) Clays, K.; Persoons, A. *Rev. Sci. Instrum.* **1992**, *63*, 3285.

(58) Firestone, K. A.; Reid, P.; Lawson, R.; Jang, S.-H.; Dalton, L. R. *Inorg. Chim. Acta* **2004**, 3957.

(59) Campo, J.; Desmet, F.; Wenseleers, W.; Goovaerts, E. *Opt. Express* **2009**, *17*, 4587.

(60) Woollam, J. A. Ellipsometry, Variable Angle Spectroscopic. In *Wiley Encyclopedia of Electrical and Electronics Engineering*; Wiley: New York, 2000; pp 109.

(61) Tian, Y.; Kong, X.; Nagase, Y.; Iyoda, T. *J. Polym. Sci., Part A: Polym. Chem.* **2003**, *41*, 2197.

(62) Tian, Y.; Akiyama, E.; Nagase, Y.; Kanazawa, A.; Tsutsumi, O.; Ikeda, T. *J. Mater. Chem.* **2004**, *14*, 3524.

(63) Kim, C.; Wallace, J. U.; Chen, S. H.; Merkel, P. B. *Macromolecules* **2008**, *41*, 3075.

(64) Bourhill, G.; Bredas, J.-L.; Cheng, L.-T.; Marder, S. R.; Meyers, F.; Perry, J. W.; Tiemann, B. G. *J. Am. Chem. Soc.* **1994**, *116*, 2619.

(65) Brown, E. C.; Marks, T. J.; Ratner, M. A. *J. Phys. Chem. B* **2008**, *112*, 44.

(66) Di Bella, S.; Marks, T. J.; Ratner, M. A. *J. Am. Chem. Soc.* **1994**, *116*, 4440.

(67) Mortazavi, M. A.; Knoesen, A.; Kowel, S. T.; Higgins, B. G.; Dienes, A. *J. Opt. Soc. Am. B* **1989**, *6*, 733.

(68) Rodriguez, V.; Adamietz, F.; Sanguinet, L.; Buffeteau, T.; Sourisseau, C. *J. Phys. Chem. B* **2003**, *107*, 9736.

(69) Kim, T.-D.; Luo, J.; Jen, A. K.-Y. *Bull. Korean Chem. Soc.* **2009**, *30*, 882.

(70) Cyvin, S. J.; Rauch, J. E.; Decius, J. C. *J. Chem. Phys.* **1965**, *43*, 4083.

(71) Oudar, J. L.; Chemla, D. S. *J. Chem. Phys.* **1977**, *66*, 2664.

(72) Oudar, J. L. *J. Chem. Phys.* **1977**, *67*, 446.

(73) In collaboration with J. A. Woollam Co., Inc., Lincoln, NE.

JP1022423